culation, the polymer chains were regarded as continuous rods. Equation 8 was used with the sums evaluated directly. Appropriate to the continuous rod model, discrete summation along a chain was replaced by integration. Because direct evaluation of the lattice sums (eq 8) was used, the results were (nonphysically) shape dependent. No *intra*molecular summation was carried out. Under this circumstance, the polarizabilities derived would be appropriate for comparison with our results for an isolated planar zigzag (Table IV). That is, the input inherent polarizability for the rod calculation (without *intra*molecular mutual induction) should be somewhat similar to that polarizability calculated for a isolated planar zigzag. Results were reported (for a spherical sample shape) of α_a = 1.90, α_b = 2.02, α_c = 5.36, and $\langle\alpha\rangle$ = 3.09 Å^3. Both the average polarizability and the anisotropy are higher than our values for the planar zigzag. Higher anisotropy could result from the fact that in the rod calculation, the polarizability is located at the rod centers, while in our calculation the centers are distributed. However, the mean value ($\langle\alpha\rangle$ = 3.09) appears to be unreasonably high compared to a vapor-phase mean polarizability increment ($\langle\alpha\rangle$ = 1.8–2.0 Å^3).

Finally, it is perhaps appropriate to comment that although polarizability is not crystal size or shape dependent, there is chain length dependence. That is, the anisotropy of an extended chain (all-trans planar zigzag) continues to increase over quite long chain lengths for finite chains. For example, the calculated contribution in our model to the molecular polarizability (isolated molecule) of the center CH_2 group in *all-trans*-pentane is α_1 = 1.58, α_2 = 1.50, and α_3 = 2.42 and for *all-trans*-heptane is α_1 = 1.55, α_2 = 1.47, and α_3 = 2.68. These are still quite far from the long chain result reported in Table IV. This effect would no doubt be ameliorated in the crystalline environment (cf. the isolated chain with the crystal result in Table IV), but it probably has some effect in the chain length region of the paraffins. A paraffin crystal is probably noticeably less anisotropic than polyethylene. a chain-folded lamellar crystal probably behaves much like a finite chain length paraffin of length similar to the lamellar thickness. For the typical lamellar thickness of 100–300 Å, the finite chain length effect is probably no longer important.

Acknowledgment. We are indebted to the Petroleum Research Fund, administered by the American Chemical Society, and to the Polymers Program, Division of Materials Research, National Science Foundation for financial support of this work.

Registry No. Methane, 74-82-8; ethane, 74-84-0; propane, 74-98-6; butane, 106-97-8; pentane, 109-66-0; hexane, 110-54-3; heptane, 142-82-5; cyclohexane, 110-82-7; polyethylene, 9002-88-4.

References and Notes

(1) Denbigh, K. G. *Trans. Faraday Soc.* **1940**, *36*, 936.
(2) Vickery, B. C.; Denbigh, K. G. *Trans. Faraday Soc.* **1949**, *45*, 61.
(3) Silberstein, L. *Phil. Mag.* **1917**, *33*, 92.
(4) Rowell, R. L.; Stein, R. S. *J. Chem. Phys.* **1967**, *47*, 2985.
(5) Applequist, J.; Carl, J. R.; Fung, K. K. *J. Am. Chem. Soc.* **1972**, *94*, 2952.
(6) Applequist, J. *J. Am. Chem. Soc.* **1973**, *95*, 8255.
(7) Applequist, J. *Acc. Chem. Res.* **1977**, *10*, 79.
(8) Ladanyi, B. M.; Keyes, T. *Mol. Phys.* **1979**, *37*, 1809.
(9) Boyd, R. H.; Kesner, L. *J. Chem. Phys.* **1980**, *72*, 2179.
(10) Boyd, R. H.; Kesner, L. *J. Polym. Sci., Polym. Phys. Ed.* **1981**, *19*, 375.
(11) Boyd, R. H.; Kesner, L. *J. Polym. Sci., Polym. Phy. Ed.* **1981**, *19*, 393.
(12) Aval, G. M.; Rowell, R. L.; Barrett, J. J. *J. Chem. Phys.* **1972**, *57*, 3104.
(13) Powers, J.; Keedy, D. A.; Stein, R. S. *J. Chem. Phys.* **1961**, *35*, 376.
(14) Dintzis, F. R.; Stein, R. S. *J. Chem. Phys.* **1964**, *40*, 1459.
(15) Bridge, N. J.; Buckingham, A. D. *Proc. R. Soc. London, Ser. A* **1966**, *295*, 334.
(16) Gucker, F. T.; Basu, S.; Pulido, A. A.; Chiu, G. *J. Chem. Phys.* **1969**, *50*, 2526.
(17) Stuart, H. A.; Schieszl, S. V. *Ann. Phys.* **1948**, *2*, 321.
(18) Buckingham, A. D.; Sutter, H. *J. Chem. Phys.* **1976**, *64*, 364.
(19) Stuart, H. A. *Landolt-Boernstein, Zahlenwerte u. Funktionen*, 6th ed.; Springer-Verlag: Berlin, 1951; Vol. I, Part 3.
(20) *Handbook of Chemistry and Physics*, 50th ed.; Chemical Rubber Co.: Cleveland, OH, 1969.
(21) Jernigan, R. L.; Flory, P. J. *J. Chem. Phys.* **1967**, *47*, 1999.
(22) Flory, P. J. *Statistical Mechanics of Chain Molecules*; Wiley Interscience: New York, 1969.
(23) Patterson, G. D.; Flory, P. J. *J. Chem. Soc., Faraday Trans. 2* **1972**, *68*, 1098.
(24) Patterson, G. D.; Flory, P. J. *J. Chem. Soc., Faraday Trans 2* **1972**, *68*, 1111.
(25) Ladanyi, B. M.; Keyes, T. *J. Chem. Phys.* **1982**, *76*, 2047.
(26) Keyes, T.; Ladanyi, B. M. *Adv. Chem. Phys.* **1984**, *56*, 411.
(27) Froehlich, H. *Theory of Dielectrics*, 2nd ed.; Oxford University Press: London, 1958.
(28) Colpa, J. H. P. *Physica* **1971**, *56*, 185.
(29) Colpa, J. H. P. *Physica* **1971**, *56*, 205.
(30) Wedgewood, A. R.; Seferis, J. C. *Polym. Eng. Sci.* **1984**, *24*, 328.
(31) Pietralla, M. *J. Polym. Sci., Polym. Phys. Ed.* **1980**, *18*, 1717.
(32) Hong, S. D.; Chang, C.; Stein, R. S. *J. Polym. Sci., Polym. Phys. Ed.* **1975**, *13*, 1447.

Study of Annealing Effects on the Structure of Vinylidene Fluoride–Trifluoroethylene Copolymers Using WAXS and SAXS

Maria Victoria Fernandez,* Atsuhiko Suzuki, and Akio Chiba

Department of Applied Physics, School of Science and Engineering, Waseda University, 3-4-1 Okubo, Shinjuku-ku, Tokyo 160, Japan. *Received December 12, 1986*

ABSTRACT: The macro- and microstructures of as-cast vinylidene fluoride–trifluoroethylene copolymers with 52/48, 54/46, and 75/25 molar compositions change remarkably with annealing temperature. The annealing effects change slightly with molar composition but may still be associated with three temperature regions: region I (cast temperatures until the ferroelectric-to-paraelectric phase transition, T_c); region II (beyond T_c until about 120–140 °C); region III (about 120–140 °C to beyond T_m). The cast films have the typical lamellar structure of crystalline polymers, with pseudohexagonal packing (low-temperature phase). For the 52/48 and 54/46 films, annealing beyond T_c creates disordering along the fiber axis but the pseudohexagonal packing remains. Near the melting temperature, a large morphological change in the lamellar structure occurs.

Introduction

Vinylidene fluoride–trifluoroethylene (VDF–TrFE) copolymers show a ferroelectric phase transition. The exact nature of this transition has been the subject of numerous researches in recent years.[1-9] It is by now recognized that the ferroelectricity of VDF–TrFE copolymers is attributed

0024-9297/87/2220-1806$01.50/0

to the fact that their crystal structure is similar to that of the piezoelectric β-phase of polyvinylidene fluoride.[8,9] Tashiro et al.[8,9] also point out that the copolymer has three crystal phases: the low-temperature and cooled phases, wherein the crystal structure is essentially equivalent to PVDF form I (β-phase), and the high-temperature phase.

Experience has discouraged the research from using as-cast (unannealed), unoriented copolymers from concentrated solution. Melting, annealing at high temperatures, drawing, poling, and high-pressure treatment of the sample are usually used. Davis et al.,[10] Lovinger et al.,[11] and Tashiro and Kobayashi[12] have made several investigations on the effect on poling and orientation on the structure of the copolymer. Ohigashi and Koga[13] show that both annealing above and poling below the ferroelectric-to-paraelectric phase transition, T_c, result in increased piezoelectric and pyroelectric activities. According to Tajitsu et al.,[14,15] the switching behavior of the copolymer changes with annealing. These facts strongly suggest that the macro- and microstructures affect ferroelectricity in the copolymer. However, the relationship between the effects of annealing and the structure of the copolymer are still not very clear.

In this study, we elucidate the effects of annealing on the structure of solution-cast, undrawn, unpoled VDF–TrFE copolymers of various molar compositions using both wide-angle (WAXS) and small-angle X-ray scattering (SAXS) techniques.

Experimental Section

The samples used were VDF–TrFE copolymers with molar contents 75/25%, 54/46% and 52/48%, which were kindly supplied by Daikin Kogyo Co., Ltd. The samples, hereafter referred to as "as cast", were cast from methyl ethyl ketone solution at room temperature for 2 weeks and were dried under vacuum. Other films were obtained by annealing at various temperatures (60–140 °C by an increment of 20 °C, finally at 155 °C) for 2 h and slowly cooling under vacuum. In this paper, what we call "melt" is 155 °C, which is beyond the melting temperature for all the samples used.

Wide- and small-angle X-ray diffraction studies were performed by using Ni-filtered Cu Kα radiation. Intensities were measured by a step by step counting method using a scintillation counter and a pulse height analyzer. Wide-angle diffraction measurements were done by the symmetrical reflection method while small-angle scattering employed the transmission technique. The small-angle scattering equipment uses a Kratky-type U-slit. The incident slit is of width 40 μm, which can measure s up to $s = 6.8 \times 10^{-4}$ Å^{-1} ($s = 2 \sin \vartheta/\lambda$). The slit's weighting function is a wide trapezoid, but the system could be regarded as an infinite slit in this experiment.

In order to take measurements in the smaller angular regions, an incident slit of width 20 μm, which can measure s up to $s = 2.267 \times 10^{-4}$ Å^{-1}, is used.

The analysis of the WAXS data was made by least-squares fitting of the peak separation method. The crystalline and amorphous peaks as well as the continuous background are identified and then separated by means of a combination of a Cauchy and a Gaussian distribution function. χ_c is computed by taking a ratio of the area integral of the crystalline and the combined crystalline and amorphous intensities, i.e., $\chi_c = \int I_c(\theta)\, d\theta / (\int I_c(\theta)\, d\theta + I_a(\theta)\, d\theta)$.

The smeared SAXS intensity $\tilde{I}$ is obtained as in the following equation: $\tilde{I} = [\tilde{I}_{obsd}{}^*(e^{-\mu t}) - \tilde{I}_{bg}] - \tilde{I}_{cb}$. Here $\tilde{I}_{obsd}$ is the observed scattering intensity for the sample and $\tilde{I}_{bg}$ is the background scattering. Both $\tilde{I}_{obsd}$ and $\tilde{I}_{bg}$ are raw data that were smoothed by using the method of splines. $\tilde{I}_{cb}$ is the constant background and its value is determined at the high-angle region wherein the resulting value for $\tilde{I}$ after the background scattering has been subtracted levels off. μ is the absorption coefficient of the sample and T is the sample thickness. The absorption coefficients of the 54/46 and 75/25 samples are $\mu_{54} = 2.06$ and $\mu_{75} = 2.05$, respectively. Each data point in the experiment represents at least 7000 counts so as to limit the error factor to ±2.4%.

All samples were not drawn and measured at room temperature.

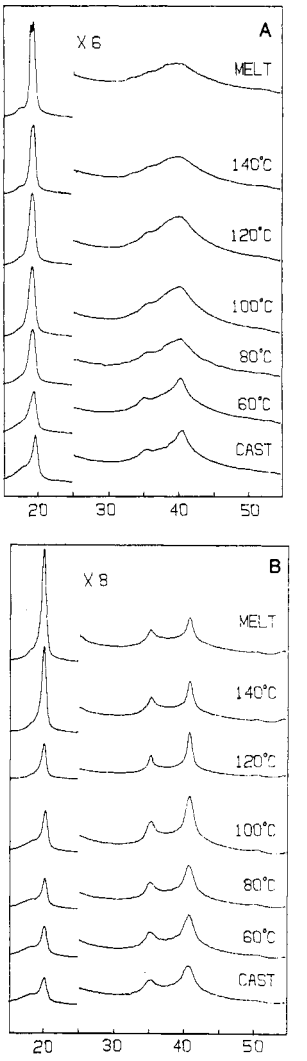

Figure 1. WAXS intensity curves for the (A) 54/46 and (B) 75/25 VDF–TrFE copolymers in the $2\vartheta \approx 19°$ and $2\vartheta \approx 35$–$40°$ regions.

Results

I. WAXS. Figure 1 shows the X-ray intensity curves for the cast, annealed, and melt samples for each composition (54/46 and 75/25 samples) in the regions 2ϑ = 15–25° and 2ϑ = 25–55°. There is a change in the WAXS curves which depends on the annealing temperature. The broad halo of the cast film around $2\vartheta \approx 18°$ that is thought to be an amorphous halo was reduced, and the intensity of the $2\vartheta \approx 19°$ peak associated with the (110) and (200) reflections increased with a rise in the annealing temperature. The peak intensity doubles in height compared to that of the cast film and eventually quadruples in height as manifested in the melt film. This is common to all the copolymer compositions used. The $2\vartheta \approx 19°$ reflection of the melt film and those annealed at 140 °C with 54/46 molar contents shows a distinct separation of two peaks. For the entire annealing process, there is no difference in the magnitude of the peak intensities in the region $2\vartheta \approx$ 30–45° associated with the (001), (111), and (201) reflections, but there exist sudden changes wherein the WAXS curves of the 54/46 samples become broad at 80 °C. The 75/25 sample, on the other hand, does not show such distinct changes. (We identified the diffraction peaks in the same way as in the crystal structure analyses of Tashiro et al.[8,9])

Figure 2 shows the results as obtained by least-squares

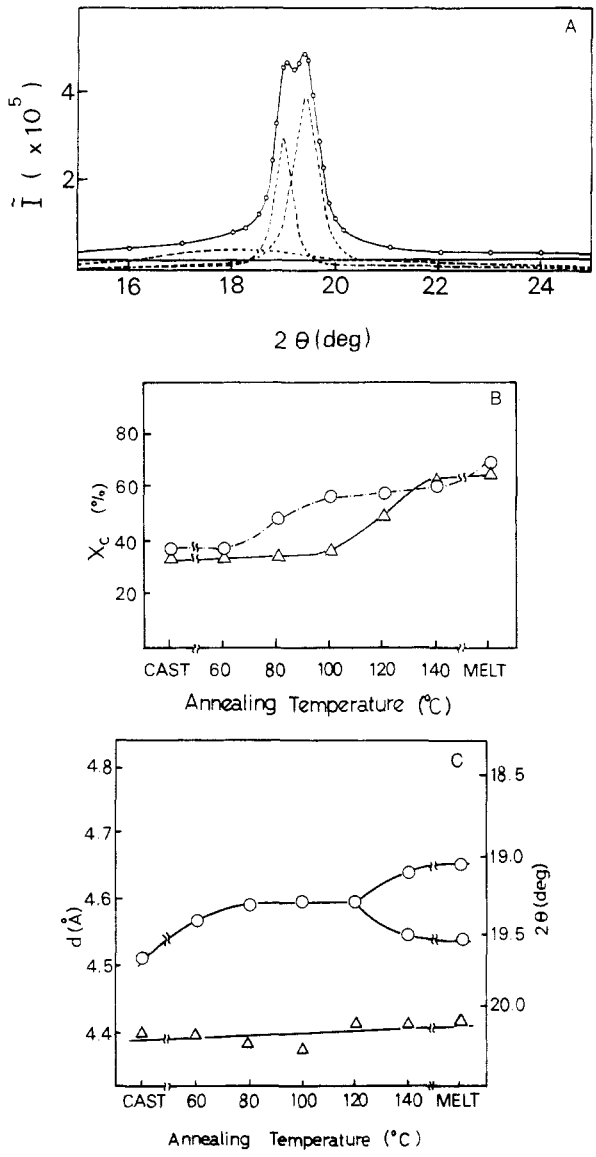

Figure 2. The results obtained by least-squares fitting of the peak separation method: (A) an example of the separation for the 54/46 VDF–TrFE melt sample (O), experimental data (---), theoretical profile as obtained by the peak separation method (—), summation of the peaks obtained by the peak separation method; (B) temperature dependence of the ratio of the crystalline and amorphous integrated intensities, χ_c (O, VDF 54; Δ, VDF 75); (C) temperature dependence of the interplanar distances d_{110} and d_{200} (O, VDF 54; Δ, VDF 75).

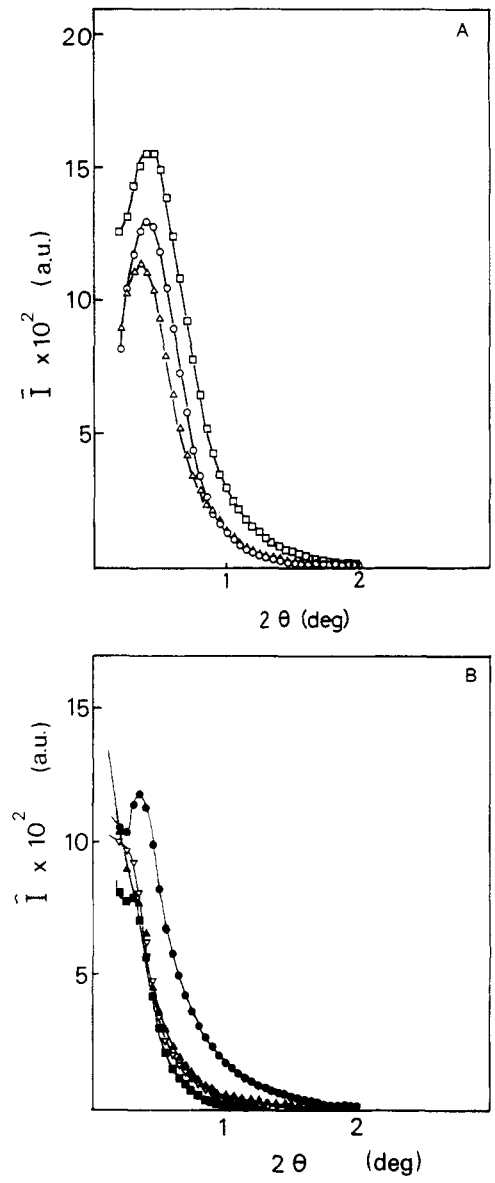

Figure 3. SAXS intensity curves for the 54/46 VDF–TrFE copolymers: (A) cast and low-temperature anneal (60–80 °C) (O, cast; □, 60 °C; Δ, 80 °C) and (B) high-temperature anneal (100–140 °C) and melt (●, 100 °C; ■, 120 °C; ▽, 140 °C; ▲, melt).

fitting of the peak separation method. Figure 2A is an example of the separation. Figure 2B shows the ratio of the crystalline and amorphous integrated intensities (referred to as χ_c), which is indicative of the sample's degree of crystallinity, as plotted against annealing temperature for each molar composition. The 54/46 sample shows an abrupt increase in χ_c at about 80 °C annealing temperature and a gradual increase in this value toward the melt temperature. The 75/25 sample, on the other hand, shows an abrupt increase in χ_c at ~120 °C after which there is only a slight increase in this value until beyond the melt temperature. The value of χ_c can be determined only with some ambiguity because when this is computed by using a Cauchy–Cauchy distribution function for the crystalline and amorphous intensities, the resulting value is about 10–20% larger than the value obtained when using a Cauchy–Gaussian distribution function. Since using a Cauchy–Gaussian distribution yields a smaller value for the standard deviation of the curve-fitting process (about 0.04%) compared to that of a Cauchy–Cauchy distribution (about 0.08%), we adopted the former.

Figure 2C shows the relationship of the interplanar distances corresponding to the diffraction peak at $2\vartheta \approx 19°$ with annealing temperature for each molar composition. The d value slightly increases with annealing temperature for the 75/25 sample. On the other hand, the 54/46 sample shows an increase in the d value from cast to melt. The d value of the 54/46 sample increases abruptly upon annealing at 60 °C whereas the χ_c value does not increase until 80 °C. Peak separation is observed at 140 °C and at the melt for this copolymer.

II. SAXS. Figure 3 shows the small-angle X-ray intensities for the 54/46 copolymer samples as plotted against s. The scattering curves for the 75/25 samples are essentially the same. For as cast films and films annealed at lower temperatures, the diffraction maxima appear (Figure 3A). At a certain temperature (~80 °C for the 54/46 films; ~120 °C for 75/25 films), the maxima shifted toward lower angles and the peaks became a bit broad with a rise in the annealing temperature. Annealing at 140 °C for the 75/25 sample as well as both the 54/46 and 75/25

Table I
Relationship of the Long Spacing, L (Å); the Degree of Crystallinity, χ_c; the Crystalline and Amorphous Peak Positions, $2\vartheta_c$ and $2\vartheta_a$, Respectively; and the Lamellar Thicknesses, d_{110}, d_{200}, d_{001}, to Annealing Temperature for the 54/46 and 75/25 VDF-TrFE Samples

	cast	60 °C	80 °C	100 °C	120 °C	140 °C	melt
				VDF 54			
L, Å	210	205	252	267	294	353	not obsd
χ_c, %	37.6	36.8	47.4	57.3	57.9	60.6	69.8
$2\vartheta_c$, deg	19.66	19.42	19.32	19.27	19.29	19.09	19.03
						19.49	19.47
$2\vartheta_a$, deg	18.43	18.43	18.62	18.58	18.57	18.34	18.17
d_{110}, Å	4.510	4.565	4.588	4.602	4.596	4.645	4.659
d_{200}, Å						4.549	4.554
d_{001}, Å	2.547	2.547	2.533	2.533	2.540	2.499	2.527
				VDF 75			
L, Å	188	205	177	205	294	not obsd	not obsd
χ_c, %	34.0	34.7	34.8	38.2	50.2	62.0	63.0
$2\vartheta_c$, deg	20.16	20.18	20.23	20.27	20.08	20.08	20.04
$2\vartheta_a$, deg	18.40	18.56	18.54	18.95	19.33	19.43	19.42
$d_{110,20}$, Å	4.401	4.402	4.385	4.375	4.417	4.417	4.426
d_{001}, Å	2.540	2.540	2.533	2.540	2.540	2.533	2.540

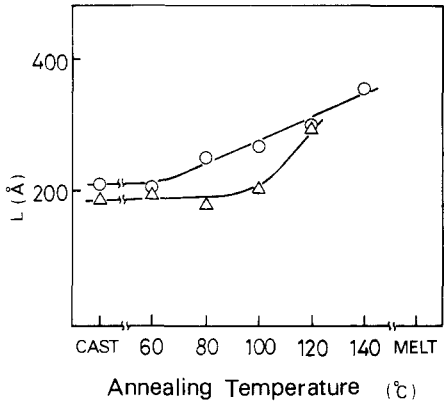

Figure 4. Temperature dependence of the long spacing, L (Å) (○, VDF 54; △, VDF 75).

melt crystallized samples does not show any peak. This behavior is shown in the relationship of the long-spacing L (Å) with the annealing temperature (Figure 4).

In order to clarify whether the diffraction peak is present in the very small angular regions of the melt films, SAXS measurements were made on the 75/25 sample using a 20-μm-wide slit system in the range $s = 1.132 \times 10^{-3}$ to 2.267×10^{-4} Å^{-1}. Results indicate that there is also no peak in this region and that $\tilde{I}(s)$ is proportional to s^{-1}.

According to Porod,[16,17] for an infinite slit system, the SAXS scattered intensity $\tilde{I}(s)$ should be proportional to s^{-3} in the high angular region for a sharp two-phase boundary structure. The relationship between log $\tilde{I}$ and log s is shown for the 75/25 sample in Figure 5. The behavior of the 52/48 and 54/46 films is essentially the same as that of the 75/25 copolymer samples. For any content, all the samples have regions with slope values of approximately -3 in the tail end of the scattering curve. Deviations from the -3 slope value occur at larger s values. Such deviations may occur due to the presence of diffuse phase boundaries between the amorphous and crystalline regions.[16-18]

Table I summarizes the behavior of the various quantities obtained by WAXS and SAXS measurements with annealing temperature for the molar compositions used.

On the basis of all the data gathered, the behavior of the 52/48 and 54/46 polymer samples is essentially the same, so that in this paper, we only present the results for the 54/46 sample.

Discussion

It has been observed that there is a change in the WAXS

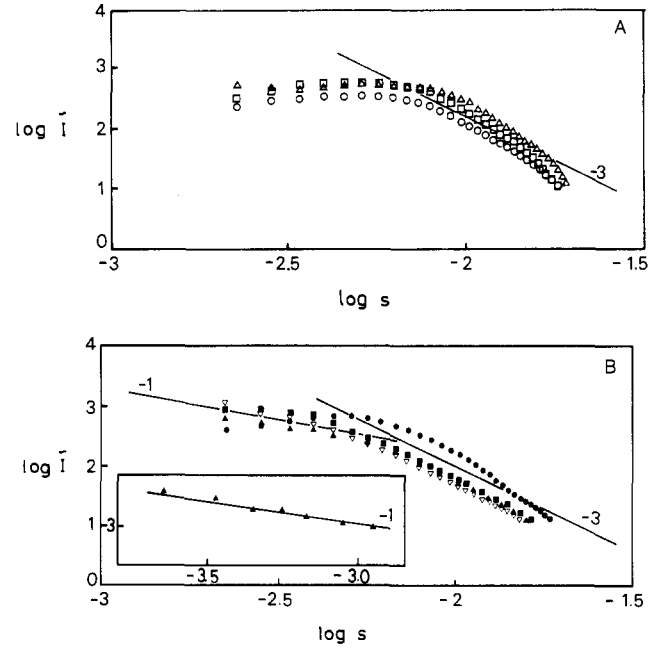

Figure 5. Plot of the logarithm of the intensity $\tilde{I}$ vs. the logarithm of s for the 75/25 VDF–TrFE copolymer: (A) cast and low-temperature anneal (60–80 °C) (○, cast; □, 60 °C; △, 80 °C); (B) high-temperature anneal (100–140 °C) and melt (●, 100 °C; ■, 120 °C; ▽, 140 °C; ▲, melt) (inset, values for the region $s = 1.132 \times 10^{-4}$ to 2.267×10^{-4} Å^{-1}).

and SAXS intensity curves of the copolymers that occurs at a specific temperature. Such an abrupt change occurs not only with the scattering intensity but also with the scattering profiles, interplanar distances, the long spacing, etc. These indicate that there is a unique temperature which signifies a structure change in the copolymers.

The 75/25 samples show changes in the vicinity of 120 °C, whereas for the 54/46 samples, changes occur at two points, at ~80 °C and in the vicinity of 140 °C. These structural changes may be attributed to two factors. One is associated with the ferroelectric to paraelectric phase transition (the temperature T_c) and the other with the melt (the temperature T_m). Since T_c and T_m are very different in value for the 54/46 copolymers ($T_c \sim 70$ °C; $T_m \sim 150$ °C), there are two different points at which a change in properties is observed in these copolymers. On the other hand, the value of T_c for the 75/25 copolymer is about 120 °C and is close to its melt temperature. Thus the changes associated with T_c are not clearly differentiated from the

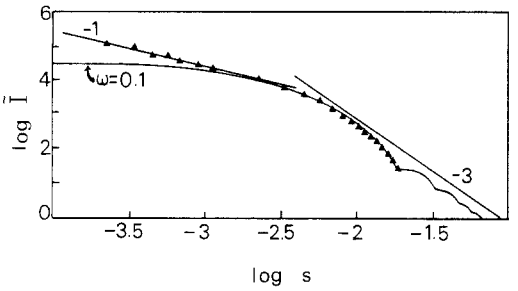

Figure 6. Comparison of the theoretical and experimental log $\tilde{I}$ vs. log s curves (experimental curve is for the 75/25 VDF–TrFE copolymer; theoretical curve makes use of a spheroid with dimensions $\omega = h/R = 0.1$; h is the semiaxis of rotation and R is the cross-sectional semiaxis).

changes associated with T_m. Even though the melt temperature is about 150 °C for all the copolymer samples, annealing in the vicinity of T_m, as well as beyond T_m, seems to produce similar effects in the copolymer's structure. The 75/25 sample was also annealed at 160 and 170 °C with very minimal changes in the observations or data produced.

These remarkable changes in the structure that accompany the annealing process may be classified into three temperature regions: region I is the temperature region from the cast temperature until T_c; region II is beyond T_c until 120–140 °C; region III is beyond 120 °C until beyond T_m. The boundary between regions II and III cannot be clearly separated, because in our experiment, annealing is done in increments of 20 °C. Experimental evidence suggests that the 120–140 °C temperature range represents a cross over between regions II and III.

Except for a large increase in the interplanar distances d_{110} and d_{200} for the 52/48 and 54/46 samples, there is very little change in the structure in region I. In this region, the films are thought to have a typical folded lamellar structure with pseudohexagonal packing (low-temperature phase).

In region II, there is an irreversible disordering along the fiber axis but this is not accompanied by a separation of the (110) and (200) peaks for the 54/46 copolymer sample. According to Tashiro et al.[8,9] annealing the VDF 55% oriented sample beyond T_c creates disordering along the fiber axis as well as separates the (110) and (200) peaks. However, our results do not show peak separation in the vicinity immediately beyond T_c. This indicates that the disordering along the fiber axis and chain packing change independently in the case of as-cast (unannealed) films. The periodic arrangement of the lamella is still present in this region.

Annealing in region III produces a SAXS intensity curve which is quite different from those of most crystalline polymers. The long spacing disappears (within the limits of our experiment, i.e., $s \geq 2.267 \times 10^{-4}$ Å^{-1}), indicating a large morphological change in the macrostructure of the copolymer. The separation of the (110) and (200) peaks for the 52/48 and 54/46 films is finally observed in this region.

We present two possible models for the interpretation of the diffuse SAXS pattern of melt crystallized samples. One is with the existence of dilute voids which developed during the annealing process and it is assumed that these voids are the origin of the dilute small-angle X-ray scattering. We tried to fit the observed data for the melt film with a theoretical scattering curve of dilute voids of the same sizes, taking into consideration various particle shapes. We found out that a spheroid would be the best shape for this model. However, we were not able to fit the theoretical and observed data closely. Comparing the theoretical curve of the plot of log $\tilde{I}$ vs. log s with the experimental curve, the part of the curve where the slope should be -1.0 is narrow for the theoretical curve (see Figure 6). Our model requires that the slope of the theoretical curve approach zero as $s \rightarrow 0$. However, the slope of the experimental curve maintains a value of −1.0 up to our experimental limit, $s = 2.267 \times 10^{-4}$ Å^{-1}. This fact suggests that the idea of void scattering is not probable. Nevertheless, it is possible to modify the model with a different void size distribution or consider a dense system so as to yield a good fit.

The other is with the existence of lamellar crystals with very long periods. This means that the scattering curve is the tail end of a diffraction peak which cannot be seen because of experimental limitations. At high annealing temperatures, there is a sudden decrease in the scattering angle 2ϑ at which the peak maxima appears, and therefore, for the melt films and the 75/25 film annealed at 140 °C, the peak is no longer observed. With this viewpoint, the structures for the copolymers annealed at high temperatures are interpreted as having lamellar structures whose long periods are no less than about 4000 Å. Such thick lamellar structures, or structures with extended chain dimensions, are known for poly(tetrafluoroethylene),[19,20] poly(chlorotrifluoroethylene),[21,22] and poly(ethylene).[23,24] The first is obtained by crystallization from the melt, the last two by crystallization from the melt under elevated pressure. The existing conditions upon growth to an extended chain are similar for both poly(tetrafluoroethylene)[20] and poly(ethylene),[23,24] i.e., there is a pseudohexagonal structure with thermal rotation about the chain axis. This condition also occurs for the VDF–TrFE copolymers in the high-temperature (hexagonal) phase.[9] While this parallelism may indicate the possibility of an extended-chain conformation in the VDF–TrFE copolymer, we still cannot make such a definitive conclusion. For oriented 75/25 VDF–TrFE copolymers, lamellar thicknesses of about 2000 Å were observed by electron microscopic studies.[25] However, there is no clear relationship between these results and our results for unoriented samples. Research regarding this problem is ongoing with the intent of clarifying the structural changes in the melt in the near future.

Recently, Tajitsu et al.[15] have indicated that switching phenomena are not observed in cast and low temperature annealed 73/27 VDF–TrFE copolymer films because of their low crystallinity, which results in high depolarization fields. Our results suggest that switching is not observed for these films not only because of their low χ_c values but also because of a large morphological change in the copolymer.

Registry No. (VDF)(TrFE) (copolymer), 28960-88-5.

References and Notes

(1) Furukawa, T.; Date, M.; Fukada, E.; Tajitsu, Y.; Chiba, A. *Jpn. J. Appl. Phys.* **1980**, *19*, L 109.
(2) Tajitsu, Y.; Chiba, A.; Furukawa, T.; Date, M.; Fukada, E. *Appl. Phys. Lett.* **1980**, *36*, 286.
(3) Kitayama, T.; Ueda, T.; Yamada, T. *Ferroelectrics* **1980**, *28*, 301; *J. Appl. Phys.* **1981**, *52*, 948.
(4) Yamada, T.; Kitayama, T. *J. Appl. Phys.* **1981**, *52*, 6859.
(5) Furukawa, T.; Johnson, G. E.; Bair, H. E.; Tajitsu, Y.; Chiba, A.; Fukada, E. *Ferroelectrics* **1981**, *32*, 61.
(6) Higashihata, Y.; Sako, J.; Yagi, T. *Ferroelectrics* **1981**, *32*, 85.
(7) Ohuchi, M.; Chiba, A.; Date, M.; Furukawa, T. *Jpn. J. Appl. Phys.* **1983**, *22*, 1267.
(8) Tashiro, K.; Takano, K.; Kobayashi, M.; Chatani, Y.; Tadokoro, H. *Polym. Prepr. Jpn.* **1981**, *30*, 654, 1878, 1882; **1982**, *31*, 2887, 2891; *32* **1983**, *32*, 860.

(9) Tashiro, K.; Takano, K.; Kobayashi, M.; Chatani, Y.; Tadokoro, H. *Polymer* **1981**, *22*, 1312; **1984**, *25*, 195; *Ferroelectrics* **1984**, *57*, 297.
(10) Davis, G. T.; Furukawa, T.; Lovinger, A.; Broadhurst, M. G. *Macromolecules* **1982**, *15*, 323, 329.
(11) Lovinger, A.; Furukawa, T.; Davis, G. T.; Broadhurst, M. G. *Polymer* **1983**, *24*, 1225, 1233; *Ferroelectrics* **1983**, *50*, 227.
(12) Tashiro, K.; Kobayashi, M. *Polymer* **1986**, *27*, 667.
(13) Ohigashi, H.; Koga, K. *Jpn. J. Appl. Phys.* **1982**, *21*, L455.
(14) Tajitsu, Y.; Date, M.; Furukawa, T.; Hantani, H.; Ogura, H.; Chiba, A. *Polym. Prepr. Jpn.* **1984**, *33*, 2587.
(15) Tajitsu, Y.; Ogura, H.; Chiba, A.; Furukawa, T. *Jpn. J. Appl. Phys.* **1987**, *26*, 554.
(16) Vonk, C. G. In *Small Angle X-ray Scattering*; Glatter, O., Kratky, A., Eds.; Applied Science: Essex, England, 1982.
(17) Porod, G. *Kolloid, Z. Z. Polym.* **1957**, *125*, 51, 108.
(18) Vonk, C. G. *J. Appl. Crystallogr.* **1973**, *6*, 81.
(19) Bunn, C. W.; Cobbold, A. J.; Palmer, R. P. *J. Polym. Sci.* **1958**, *28*, 365.
(20) Matsushige, K.; Enoshita, R.; Ide, T.; Yamauchi, N.; Taki, S.; Takemura, T. *Jpn. J. Appl. Phys.* **1977**, *16*, 681.
(21) Wunderlich, B.; Arakawa, T. *J. Polym. Sci., Part A* **1964**, *1*, 1245.
(22) Geil, P. H. *J. Polym. Sci. Part A* **1964**, *2*, 3813.
(23) Miyamoto, Y.; Nakafuku, C.; Takemura, T. *Polym. J.* **1972**, *3*, 120.
(24) Bassett, D. C. In *Developments in Crystalline Polymers-1*; Bassett, D. C., Ed.; Applied Science: Essex, England, 1982.
(25) Ohigashi, H.; Koga, K.; Suzuki, M.; Nakanishi, T.; Kimura, K.; Hashimoto, N. *Ferroelectrics*. **1984**, *60*, 263.

Polymer Scission with Irreversible Reattachment: A Kinetic Model of Pyrolysis with Char Formation

Alan R. Kerstein*

Sandia National Laboratories, Livermore, California 94550

Stephen Niksa

High Temperature Gasdynamics Laboratory, Mechanical Engineering Department, Stanford University, Stanford, California 94305. *Received November 17, 1986*

ABSTRACT: The pyrolitic degradation of polymers is modeled by the simultaneous processes of bond scission and irreversible monomer reattachment applied to linear chains or branching (loopless) networks. The monomer, or elemental unit, of the network is assumed to be the common precursor of volatiles (tar), formed by a first-order rate process, and refractory solids (char), formed by monomer reattachment to any broken bond. A closed set of rate equations governing this model is derived. Exemplary cases are solved, and a previous application of this model to coal devolatilization is discussed. The predicted dependence of tar and char yields on heating rate, a consequence of network statistics in conjunction with temperature-dependent reaction rates, is consistent with devolatilization measurements and may be relevant to other pyrolysis processes. The network version of the model exhibits a percolation transition which may represent the softening transition observed during the pyrolysis of some coals.

1. Introduction

Recent analyses of polymer degradation kinetics have focused primarily on two issues. First, the steady-state size distribution has been analyzed for polymers subject to simultaneous scission and reattachment processes, with both processes reversible.[1,2] Second, the complete transient evolution has been analyzed for a class of linear-chain models of polymers subject to irreversible scission with no reattachment.[3] Here we consider the complete transient evolution of a class of linear-chain and branching (loopless) network models subject to scission with irreversible reattachment.

The analysis is motivated by certain features of pyrolysis processes in which volatiles (tar) and refractory solids (char) are produced. As a concrete example, we consider the application to coal devolatilization that originally motivated the analysis.[4] Transient and ultimate tar and char yields during the thermal decomposition of coal have traditionally been modeled by postulating a small number of species classes, or lumps, in the unreacted coal which react according to a simple chemical-kinetic scheme. These lumps are converted to product either directly or through a reactive intermediate (metaplast) according to a scheme with phenomenologically assigned stoichiometric coefficients and temperature-dependent (typically Arrhenius) rate coefficients.

Motivated by recent progress in the development of a macromolecular picture of coal structure,[5] we have formulated[4] a pyrolysis model in which the reactive intermediate is the elemental unit (monomer) in a network representing the unreacted coal. Pyrolytic decomposition is represented by scission of network bonds. After an individual monomer is freed, i.e., fully detached from its neighbors, it is subject to two competing processes. One process is conversion to tar (which escapes from the system) according to a first-order rate process. The other process is irreversible reattachment to any broken bond. The irreversible nature of this reattachment reflects the refractory nature of the char which is formed during pyrolysis. The stability of the reattached bonds results in inhibition of the rate of free monomer release for a given bond-scission rate. This inhibition introduces a dynamic feedback effect of char formation on the production of free monomers. The quantitative impact of this feedback, which is governed by the statistics of network fragmentation, is the key feature of the model which has led to an enhanced capability to predict heating-rate dependences of transient and ultimate yields measured over a wide range of experimental conditions.[6-8]

The previously presented formulation[4] of our network model of pyrolysis incorporated additional features, such as dangling side branches, intended to represent aspects

0024-9297/87/2220-1811$01.50/0